



# Modeling mechanical response and texture evolution of $\alpha$ -uranium as a function of strain rate and temperature using polycrystal plasticity

Marko Knezevic\*, Rodney J. McCabe, Carlos N. Tomé, Ricardo A. Lebensohn, Shuh Rong Chen, Carl M. Cady, George T. Gray III, Bogdan Mihaila

Materials Science and Technology Division, Los Alamos National Laboratory, Los Alamos, NM 87545, USA

## ARTICLE INFO

### Article history:

Received 10 August 2012

Received in final revised form 26 October 2012

Available online 15 November 2012

### Keywords:

A. Anisotropic material

A. Microstructures

A. Twinning

B. Rate-dependent material

B. Temperature-dependent material

## ABSTRACT

We present a polycrystal plasticity model based on a self-consistent homogenization capable of predicting the macroscopic mechanical response and texture evolution of  $\alpha$ -uranium over a wide range of temperatures and strain rates. The hardening of individual crystals is based on the evolution of dislocation densities and includes effects of strain rate and temperature through thermally-activated recovery, dislocation substructure formation, and slip-twin interactions. The model is validated on a comprehensive set of compression tests performed on a clock-rolled  $\alpha$ -uranium plate at temperatures ranging from 198 to 573 K and strain rates ranging from  $10^{-3}$  to  $3600 \text{ s}^{-1}$ . The model is able to reproduce the stress-strain response and texture for all tests with a unique set of single-crystal hardening parameters. We elucidate the role played by the slip and twinning mechanisms and their interactions in large plastic deformation of  $\alpha$ -uranium as a function of strain rate and temperature.

© 2012 Elsevier Ltd. All rights reserved.

## 1. Introduction

Uranium and uranium alloys are nuclear material systems important for defense-related and energy applications including metallic nuclear fuels. These materials usually have low-symmetry crystal structures and exhibit complex deformation behavior. During manufacturing and in service, these materials may be subject to high temperature and/or high strain rate conditions. Predicting the material behavior and microstructure evolution during processing and service requires material models that account for temperature and strain rate effects. The accuracy of such models is particularly important for nuclear materials where operating conditions and material hazards may limit the ability to perform experiments to evaluate the material behavior.

The room-temperature allotrope of uranium metal,  $\alpha$ -uranium ( $\alpha$ -U), is stable up to 940 K and has an orthorhombic crystal structure. Due to its low-symmetry crystal structure, the deformation behavior of  $\alpha$ -U single crystal exhibits strong anisotropy. Polycrystalline aggregates of  $\alpha$ -U are also highly anisotropic due to pronounced texture (non-random distribution of crystallographic orientations) introduced by thermo-mechanical processing.  $\alpha$ -U deforms by a wide variety of plastic deformation mechanisms with considerably different activation stresses, and these activation stresses evolve differently with deformation making the evolution of macroscopic hardening also highly anisotropic. Studies of the deformation mechanisms of single-crystal  $\alpha$ -U and the mechanical response of  $\alpha$ -U aggregates date back over 50 years (Anderson and Bishop, 1962; Cahn, 1951, 1953; Daniel et al., 1971; Fisher and McSkimin, 1958). The dislocation glide and deformation twinning modes accommodating plastic strains were identified and their relative strengths were measured for single crystals. It

\* Corresponding author. Tel.: +1 505 665 7587; fax: +1 505 667 8021.

E-mail address: [knezevic@lanl.gov](mailto:knezevic@lanl.gov) (M. Knezevic).

was established that the easiest slip mode in  $\alpha$ -uranium is (010)[100] (Daniel et al., 1971; Yoo, 1968). The (001)[100] slip mode was found to become the predominant slip mode at elevated temperatures (Daniel et al., 1971; Yoo, 1968). It is important to note that both slip modes contain only one independent slip system. The  $1/2\{110\}\langle 1\bar{1}0\rangle$  slip mode also operates, but requires a higher driving force than the primary (010)[100] slip mode (Daniel et al., 1971). The  $1/2\{1\bar{1}2\}\langle 021\rangle$  slip mode offers the additional degree of freedom necessary to accommodate plastic strain in the [001] direction and, thus, to accommodate an arbitrary plastic strain. In addition to slip, these studies reported the occurrence of deformation twinning in  $\alpha$ -U. The most prominent deformation twin was found to be the  $\{130\}\langle 3\bar{1}0\rangle$  twin mode (Cahn, 1951, 1953; Daniel et al., 1971). The  $\{172\}\langle 3\bar{1}2\rangle$  twin mode and its reciprocal twin,  $\{112\}\langle 3\bar{7}2\rangle$ , were also frequently observed (Cahn, 1951, 1953; Crocker 1965; Daniel et al., 1971). Illustrations of  $\alpha$ -U crystal structure and slip and twinning system geometries can be found in McCabe et al. (2010).

Early attempts at modeling and characterization of crystallographic texture in  $\alpha$ -U sample took place in the 1950s (Calnan and Clews, 1952; Mitchell and Rowland, 1954). More recent attempts to model texture evolution during rolling of  $\alpha$ -U were reported in the early 1990s (Lebensohn and Tomé, 1994; Rollett, 1991) using the relative strength of the deformation modes reported in Daniel et al. (1971). The advent of new experimental characterization techniques such as electron backscattered diffraction (EBSD) (Knezevic et al., 2012; McCabe et al., 2010; McCabe and Teter, 2006) and neutron diffraction (Brown et al., 2009; Choi and Staker, 1996), together with the development of new modeling techniques (Knezevic et al., 2012; McCabe et al., 2010), have created new interest in performing detailed studies aimed at understanding the basic behavior of uranium. Recently, we presented a comprehensive quantitative analysis focused on the room temperature quasi-static mechanical response and concomitant texture evolution of  $\alpha$ -U with initial clock-rolled, straight rolled, and swaged textures (Knezevic et al., 2012). The insight obtained from these extensive experimental data sets were incorporated in a multi-scale hardening law based on dislocation densities which was implemented in the visco-plastic self-consistent (VPSC) model to predict the anisotropic stress–strain response and texture evolution of  $\alpha$ -U (Knezevic et al., 2012; McCabe et al., 2010). Comparison of simulations and experiments allowed for inference of basic information concerning the various slip and twin mechanisms, their interactions, and their role on strain hardening and texture evolution. It was found that the initial texture plays a significant role in determining the level of plastic anisotropy, and deformation twinning plays a major role in anisotropic strain hardening behavior, tension–compression asymmetry and texture evolution in  $\alpha$ -U (Knezevic et al., 2012; McCabe et al., 2010). Hence, it was evident that the accurate modeling of this complex material system requires a crystal-plasticity theoretical framework that accounts for microstructure evolution, rather than a continuum approach.

In this paper, we extend the hardening law based on dislocation densities and report the first microstructure-based model which includes strain-rate and temperature effects on deformation behavior of uranium. The enhanced predictive capabilities of this model will allow us to tackle simulations of complex forming operations of  $\alpha$ -U. We calibrate and validate our model against new experimental data. Our model takes advantage of previous studies of strain-rate and temperature dependence of low-symmetry metals such as zirconium (Beyerlein and Tomé, 2008; Song and Gray, 1995a), titanium (Gray, 1997), magnesium (Barnett, 2001; Basinski, 1960), and beryllium (Brown et al., 2012). For those materials, twinning also plays a major role in deformation and studies have confirmed that increases in strain rate and decreases in temperature increase activity of deformation twinning through suppression of thermally-activated dislocation glide processes. Prior to the present study, the influence of temperature and strain rate on the mechanical behavior of uranium has received much less attention: a systematic investigation of the influence of temperature on the critical resolved shear stress for all four slip modes on single crystals of  $\alpha$ -U was reported in Daniel et al. (1971) and some theoretical calculations of Peierls–Nabarro stress for (010) and (001) edge dislocations as a function of temperature were given in Yoo (1968).

We begin by presenting a large set of mechanical testing data performed on samples machined from an annealed clock-rolled plate of  $\alpha$ -U. The mechanical tests were performed at temperatures ranging from 198 to 573 K and under strain rates ranging from  $10^{-3}$  to  $3600\text{ s}^{-1}$ . Subsequently, we discuss the hardening law implemented in VPSC, with an emphasis on details necessary for understanding the deformation mechanisms at various deformation conditions. Then, we calibrate and validate the model against the comprehensive set of rate and temperature-sensitive mechanical data. We show that the model is able to reproduce the stress–strain response for all tests with a unique set of single-crystal hardening parameters. These predictions allow us to elucidate the role played by the deformation mechanisms and their interactions in large plastic deformation and texture evolution of  $\alpha$ -U as a function of strain rate and temperature. Strong shifts in the relative contribution of active deformation modes are observed when different deformation conditions are applied and these results will be discussed in detail.

## 2. Material and experiments

The material discussed here is clock-rolled  $\alpha$ -U plate. The processing route was described earlier (Knezevic et al., 2012; McCabe et al., 2010). Samples were machined from the plate and annealed at 820 K for 2 h before testing. The microstructure and texture of the material before testing are shown in Fig. 1. The orientation map shows equiaxed twin-free grains with an average grain size of about  $15\ \mu\text{m}$ . The processing route of the starting material induced an orthotropic texture, which allows us to show only one quarter of the pole figures. The pole figures reveal that the material has a strong (001) texture component in the through-thickness (TT3) direction, tilted towards the in-plane 2 (IP2) direction. The (010) and (100) components tend to concentrate away from the (TT3) direction with the peak intensity for (010) being in the in-plane 1 (IP1) direction

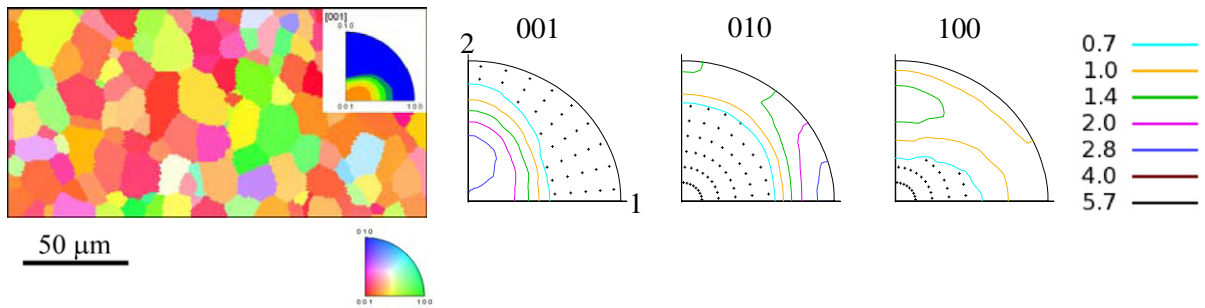


**Fig. 1.** EBSD orientation map and pole figures showing initial microstructure and texture in the as-annealed sample of clock-rolled uranium. The colors in the map indicate the crystal direction parallel to the TT3 direction (unit triangle at the bottom). In the corner of the map we illustrate the inverse pole figure for the TT3 direction. The IPF triangle has the crystal reference frame defined as [100] to the right, [010] upward, and [001] in the center. The IP1 and IP2 directions are indicated by the 1 and 2 on the pole figures.

and the peak intensity for (100) being at about  $60^\circ$  from the TT3 direction towards IP2. Here, IP1 is the direction parallel to the final rolling direction and IP2 is the direction transverse to the final rolling direction.

### 2.1. Mechanical testing at room temperature under quasi-static loading

Compression samples were machined as right circular cylinders in the IP1, IP2 and TT3 directions, with either 5 or 6.35 mm diameters. The samples are grouped and presented according to the macroscopic deformation mode to be imposed using the following conventions: IPC1, IPC2, and TTC3. Constant velocity compression tests were performed at nominal strain rates of  $10^{-1}$ ,  $10^{-2}$ , and  $10^{-3} \text{ s}^{-1}$  at room temperature using a screw-driven Instron. Polished tungsten carbide platens were used to load the compression samples lubricated with molybdenum disulfide grease to reduce frictional effects. The raw data was collected in the form of load–displacement curves and was corrected for machine compliance before computing the true stress–true strain curves.

### 2.2. Mechanical testing at various temperatures and strain rates

The mechanical responses of the uranium plates were measured in compression using solid-cylindrical samples 5 mm in diameter by 5 mm long, lubricated with molybdenum disulfide grease. Compression samples were machined from the plates in both the TT3 and IP2 longitudinal orientations. Quasi-static compression tests were conducted at several temperatures under strain rates of  $10^{-3}$  and  $10^{-1} \text{ s}^{-1}$ . A hot stage with heated platens was designed to probe the temperature sensitivity of the material. Dynamic tests at strain rates of  $2000\text{--}4000 \text{ s}^{-1}$  were conducted at room temperature utilizing a Split-Hopkinson Pressure Bar (Chen and Kocks, 1991; Follansbee, 1985).

### 2.3. Mechanical testing results

The measured compressive stress–strain response of  $\alpha$ -U as a function of strain rate and temperature is shown in Fig. 2. We find that the yield and flow stresses of  $\alpha$ -U are sensitive to changes in temperature and strain rate. There is significant anisotropy between compression in the TT and IP directions. Despite small differences in the initial texture with respect to the IP1 and IP2 directions, the compressive response along these two directions at room temperature and under quasi-static strain rate is similar. For this reason, we test the temperature and high strain-rate effects along the IP2 and TT directions.

We first examine the quasi-static response at different temperatures. The anisotropy between the TT and IP compressed samples is most pronounced at 198 K, but still present even at 573 K. The work hardening rate at 198 K for the IP compressed samples is significantly higher than that of the TT compressed sample. The increasing work hardening rate of the IP curve is typical of deformation twinning activity (Knezevic et al., 2012), as will be supported with the microstructure data in the results section. The TT response exhibits a classical decreasing hardening rate throughout, which is a sign that the plastic deformation is dominated by slip. The decrease of the hardening rate during the TT compression is more pronounced with increasing temperature due to the thermal activation of dislocation slip. The strain-hardening rates for IP and TT compression are similar at 573 K, where thermally-activated processes become easier.

We now turn our attention to the room temperature response under different strain rate conditions. The work hardening rate during IP compression is higher at high strain-rate conditions especially in the early portion of the stress strain curve relative to the quasi-static loading conditions. We hypothesize that the increase in the hardening rate under higher strain-rate relative to quasi-static conditions is due to a combination of more difficult thermally-activated slip and stronger slip-twin interactions, as will be discussed in the next section. The macroscopic initial yield stress appears insensitive to the rate of deformation in the IP compression direction. Both the macroscopic initial yield stress and the initial macroscopic hardening rate appear to increase with the rate of deformation for TT compression. We associate these increases with the sensitivity of dislocation slip to the rate of plastic deformation. We note that most of the deformation in the TT compression

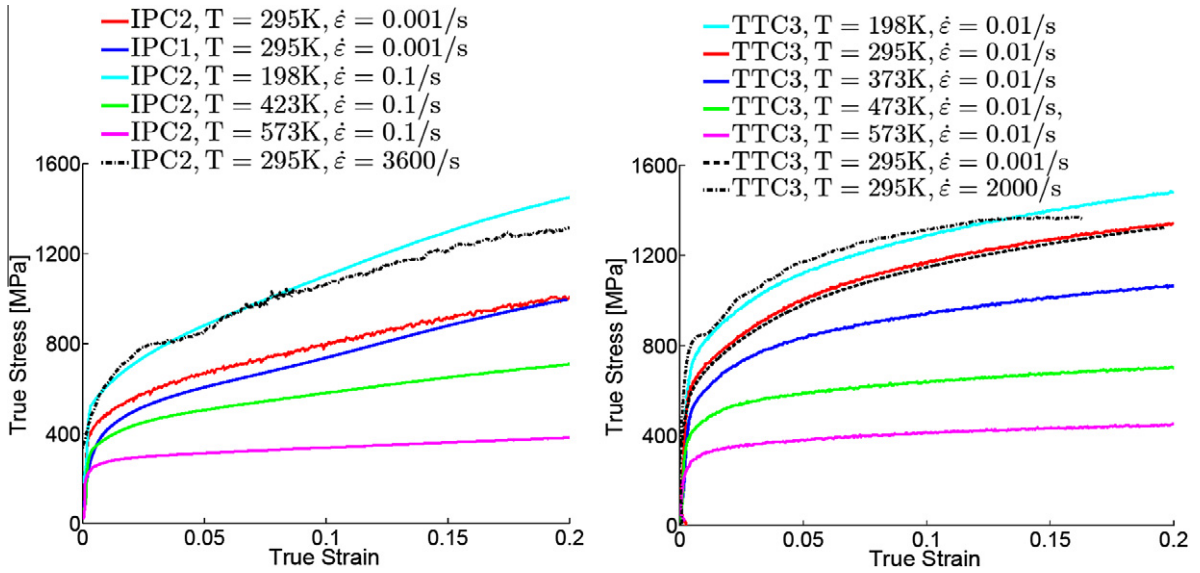


Fig. 2. Measured stress–strain response in compression on annealed samples of  $\alpha$ -uranium along the directions and at the temperate and strain rate indicated in the plots.

is accommodated by dislocation slip, which is a thermally-activated process. These processes are more difficult to activate if strain rate increases or if temperature decreases, and are likely responsible for the increase of the macroscopic initial yield stress and work hardening in the TT compressed samples. Generally, thermally-activated processes become prevalent after some amount of straining. It is seen that the work hardening rate of the TT compressed sample under a high strain rate tends to saturate faster than under quasi-static conditions.

The influence of the deformation mechanisms and their interactions on the mechanical response of  $\alpha$ -U will be interpreted using the polycrystal plasticity model presented in the next sections.

### 3. Modeling framework

To model the mechanical behavior of polycrystalline  $\alpha$ -U, we use a mean-field, self-consistent model based on the solution of the deformation of an ellipsoidal inclusion embedded in a homogenous effective medium, both exhibiting an anisotropic response. The inclusion is taken to be an individual grain, while the homogenous medium represents the polycrystalline aggregate. A detailed description of the visco-plastic self-consistent (VPSC) model used in this study can be found elsewhere (Lebensohn and Tomé, 1993; Lebensohn et al., 2007). Because the VPSC scheme captures the relative directional anisotropy of inclusion and medium, it is particularly appropriate for modeling highly anisotropic crystals, such as  $\alpha$ -U. The temperature and rate-dependent single-crystal dislocation-density-based hardening law was reported earlier in Beyerlein and Tomé (2008), Knezevic et al. (2012) and McCabe et al. (2010). The law links the threshold stresses for slip and twin activation, with the current dislocation density in each of the slip modes. The underlying equations of the hardening law are presented below with an emphasis on the modifications needed to capture the temperature and strain rate effects on the mechanical response of  $\alpha$ -U.

The plastic deformation in each grain occurs via the activation of slip and twin systems. The corresponding slip or twin shear strain rate,  $\dot{\gamma}^s$  on a given system,  $s$ , is related to the stress in the grain (inclusion) using the power-law relation:

$$\dot{\gamma}^s = \dot{\gamma}_0 \left| \frac{\tau^s}{\tau_c^s} \right|^{\frac{1}{m}} \text{sign}(\tau^s). \quad (1)$$

Here,  $\dot{\gamma}_0$ ,  $m$ ,  $\tau^s$ , are a reference shear rate, rate sensitivity parameter, and resolved shear stress in the system, respectively.  $\tau_c^s$  is the threshold stress for activating the slip or twin system, and its dependence with temperature, rate and dislocation density is the focus of this work. The twin propagation is treated as a pseudo-slip mechanism, as originally proposed in Van Houtte (1978). The propagation i.e. evolution of twin volume fraction is obtained by time integration of the ratio of the shear rate on a twin system  $s$  and the inherent twinning shear  $\int \dot{\gamma}^s / \gamma^{tw} dt = f^s$ . The  $\{130\}\langle 3\bar{1}0\rangle$  and  $\{172\}\langle 3\bar{1}2\rangle$  twins have twinning shears of 0.299 and 0.227, respectively. Consistent with experimental evidence and our earlier studies, the following slip modes  $(010)[100]$ ,  $(001)[100]$ ,  $1/2\{110\}\langle 1\bar{1}0\rangle$  and  $1/2\{1\bar{1}2\}\langle 021\rangle$  and twin modes  $\{130\}\langle 3\bar{1}0\rangle$  and  $\{172\}\langle 3\bar{1}2\rangle$  are considered as potential systems for accommodating the imposed plastic strain. The parameter  $m$  is taken to be  $m = 0.05$  for slip and twinning, and does not represent the rate sensitivity of the system. Rather, the rate dependence is accounted for explicitly by

the functional form of  $\tau_c^s$ . Computationally, we eliminate the rate sensitivity that is introduced via  $m$  by setting the reference shear rate  $\dot{\gamma}_0$ , equal to the norm of the macroscopic strain rate  $= \dot{\gamma}_0 = \|\dot{\bar{\epsilon}}\|$ . If  $\sigma'_{kl}$  is the stress that induces a rate  $\dot{\epsilon}_{ij}$  in the grain when  $\bar{\epsilon}$  is applied, the relation between these magnitudes is given by the rate equation

$$\dot{\epsilon}_{ij} = \|\bar{\epsilon}\| \left\| \sum_s S_{ij}^s \left( \frac{S_{kl}^s \sigma'_{kl}}{\tau_c^s} \right)^{\frac{1}{m}} \right\|, \quad (2)$$

where the sum runs over all slip and twin systems and  $S_{kl}^s$  is the Schmid tensor associated with slip or twinning system  $s$ . If a rate  $\lambda \bar{\epsilon}$  is applied, the rate  $\dot{\epsilon}_{ij}$  in the grain is given by

$$\dot{\epsilon}_{ij} = \|\lambda \bar{\epsilon}\| \left\| \sum_s S_{ij}^s \left( \frac{S_{kl}^s \sigma'_{kl}}{\tau_c^s} \right)^{\frac{1}{m}} \right\|, \quad (3)$$

where the stress  $\sigma'_{kl}$  is the same, provided that the threshold stress  $\tau_c^s$  does not change with rate.

All slip systems or twin variants within one mode  $\alpha$  (or family) in a grain are assumed to exhibit the same resistance. The evolution of the resistance for each slip and twinning modes is based on individual strain rate and temperature dependencies and on their interactions.

For slip, the resistance is expressed as a sum of an initial slip resistance  $\tau_0^\alpha$  (Peirls, precipitates, initial debris), a forest dislocation interaction stress  $\tau_{for}^\alpha$ , and a dislocation substructure interaction stress  $\tau_{sub}^\alpha$ , i.e.

$$\tau^\alpha(\dot{\epsilon}, T) = \tau_0^\alpha(T) + \tau_{for}^\alpha(\dot{\epsilon}, T) + \tau_{sub}^\alpha(\dot{\epsilon}, T). \quad (4)$$

The initial slip resistances  $\tau_0^\alpha(T)$  for all four slip modes were shown to decay exponentially with temperature for uranium (Daniel et al., 1971; Yoo, 1968). Such exponential-decay expressions were also used for other low-symmetry metals including magnesium, zirconium, and beryllium (Beyerlein and Tomé, 2008; Flynn et al., 1961). Therefore, we adopt the following form of the equation for the initial slip resistance per slip mode:

$$\tau_0^\alpha(T) = A^\alpha \exp\left(-\frac{T - T_{ref}}{B^\alpha}\right), \quad (5)$$

where  $A^\alpha$  and  $B^\alpha$  are constants, whereas  $T$  and  $T_{ref}$  are the current and reference temperatures, respectively. The latter is taken as the room temperature. The evolution of  $\tau_{for}^\alpha$  and  $\tau_{sub}^\alpha$  is governed by the evolution of the forest  $\rho_{for}^\alpha$  and substructure  $\rho_{sub}$  dislocation densities. The effect of forest dislocation density is given by a modified Taylor law relationship:

$$\tau_{for}^\alpha = b^\alpha \mu^\alpha(T) \sqrt{\chi^{\alpha\alpha'} \rho_{for}^{\alpha'}}, \quad (6)$$

where  $\chi^{\alpha\alpha'}$  is a dislocation interaction matrix. Unlike earlier work, where we used a scalar  $\chi$  parameter and only the dislocation density of the corresponding slip mode in the Taylor relationship, here we couple the dislocation densities of all modes via the interaction matrix  $\chi^{\alpha\alpha'}$ . This is particularly important for uranium because this material features slip modes containing only one slip system. The influence of interactions between different modes is reflected by the off-diagonal components of the matrix  $\chi^{\alpha\alpha'}$ . The magnitude of the  $\chi$  parameter was reported to be in the range 0.05–2.6 and dependent on crystal structure, temperature, strain rate and alloying (Lavrentev, 1980). An analysis of earlier studies shows there is no complete agreement as to whether the parameter increases or decreases with temperature and strain rate. For this reason and for simplicity, we decided to treat the parameter as independent on temperature and strain rate. Dislocation dynamics simulations show that the contribution to hardening by dislocations stored within substructures can be given as (Madec et al., 2002)

$$\tau_{sub}^\alpha = k_{sub} b^\alpha \mu^\alpha(T) \sqrt{\rho_{sub}} \log\left(\frac{1}{b^\alpha \sqrt{\rho_{sub}}}\right). \quad (7)$$

Here,  $k_{sub} = 0.086$  is an empirical parameter that recovers the Taylor law for low substructure dislocation densities (Madec et al., 2002). We note that Eq. (7) takes into account the latent hardening effects between slip systems implicitly through the substructure dislocations arising from the effects of imperfect recovery on all slip systems within the grain, rather than by including those dislocations in Eq. (6).

The evolution of the stored forest density  $\rho_{for}^\alpha$  is governed by competition between the rate of storage and the rate of dynamic recovery:

$$\frac{\partial \rho_{for}^\alpha}{\partial \gamma^\alpha} = \frac{\partial \rho_{gen,for}^\alpha}{\partial \gamma^\alpha} - \frac{\partial \rho_{rem,for}^\alpha}{\partial \gamma^\alpha} = k_1^\alpha \sqrt{\rho_{for}^\alpha} - k_2^\alpha(\dot{\epsilon}, T) \rho_{for}^\alpha, \quad (8)$$

where  $k_1^\alpha$  is a rate-insensitive coefficient for dislocation storage by statistical trapping of mobile dislocations and  $k_2^\alpha$  is a rate-sensitive coefficient that accounts for dynamic recovery by thermally-activated mechanisms. The latter coefficient,  $k_2^\alpha$ , is given by Beyerlein and Tomé (2008)

$$\frac{k_2^\alpha}{k_1^\alpha} = \frac{\chi b^\alpha}{g^\alpha} \left(1 - \frac{kT}{D^\alpha b^3} \ln\left(\frac{\dot{\epsilon}}{\dot{\epsilon}_0}\right)\right). \quad (9)$$

In Eq. (9),  $k$ ,  $\dot{\epsilon}_0$ ,  $g^\alpha$ , and  $D^\alpha$  are, respectively, the Boltzmann constant, a reference strain rate (taken to be  $10^7 \text{ s}^{-1}$ ), an effective activation enthalpy and a drag stress. Dynamic recovery is often associated with thermal activation of dislocation cross-slip and climb, and the formation of dislocation substructures is concomitant with these recovery processes. As a consequence, the rate of substructure development is coupled with the rate of recovery of all active dislocations through:

$$d\rho_{sub} = \sum_{\alpha} q^{\alpha}(T) b^{\alpha} \sqrt{\rho_{sub}} \frac{\partial \rho_{rem,for}^{\alpha}}{\partial \gamma^{\alpha}} d\gamma^{\alpha}, \quad (10)$$

where  $q(T)$  is an  $\alpha$ -type dislocation recovery rate coefficient defining the fraction of dislocations that do not annihilate but become substructure. The rate of substructure formation is expected to decrease with temperature as more dislocations tend to annihilate. We vary the recovery rate coefficient with temperature using:

$$q^{\alpha}(T) = C^{\alpha} \exp\left(-\frac{T - T_{ref}}{E^{\alpha}}\right), \quad (11)$$

where  $C^{\alpha}$  and  $E^{\alpha}$  are constants characteristic of each slip mode.

The resistance for twin activation accounts for a temperature-independent friction term  $\tau_0^{\beta}$  and a latent hardening term coupling slip and twin systems. The evolution of the critical resolved shear stress for twinning is given by

$$\tau_c^{\beta}(\dot{\epsilon}, T) = \tau_0^{\beta} + \mu^{\beta} \sum_{\beta} C^{\alpha\beta}(\dot{\epsilon}) b^{\beta} b^{\alpha} \rho_{for}^{\alpha}(\dot{\epsilon}, T). \quad (12)$$

Here,  $\mu^{\beta}$ ,  $b^{\beta}$  and  $C^{\alpha\beta}$  are the elastic shear modulus on the system, the Burgers vector of a twin given system, and the latent hardening matrix, respectively. We include the rate effects in the latent hardening matrix  $C^{\alpha\beta}$  based on our hypothesis that the strength of the slip-twin interactions is expected to vary with strain rates. At higher strain rates, twinning is more active and grains may contain sets of thin twins (Song and Gray, 1995b). These morphological features of twins coupled with the increased number of dislocation sources created at higher strain rates is expected to increase the strength of the slip-twin interactions. We model these effects using:

$$C^{\alpha\beta}(\dot{\epsilon}) = F^{\alpha\beta} \exp\left(\frac{\dot{\epsilon} - \dot{\epsilon}_{ref}}{G^{\alpha\beta}}\right), \quad (13)$$

where  $F^{\alpha\beta}$  and  $G^{\alpha\beta}$  are constants characteristic of each twin mode and  $\dot{\epsilon}$  and  $\dot{\epsilon}_{ref} = 0.001$  are the current strain rate and a reference strain rate, respectively.

The twin transformation is modeled using a version of the Composite Grain (CG) model in which matrix and twin are treated as uncoupled lamellae (Proust et al., 2009) instead of enforcing continuity conditions across the twin-matrix interface (Proust et al., 2007). In brief, the twin system with the highest shear-rate among all active twin systems (Predominant Twin System, PTS) in each grain is identified, and the grain is partitioned into a stack of flat ellipsoids with the crystallographic orientation of the PTS and the matrix. The number of these flat ellipsoids, and thus the thickness of the twins, is a variable in our model. At low strain rates we allow nucleation of two twins per grain while at high strain rates we allow nucleation of up to five twins per grain. The short axis of the ellipsoids is perpendicular to the twin plane. As more shear is accommodated by twinning, a volume fraction is transferred from the parent to the twin: the ellipsoids representing the twins thicken and the ones representing the parent shrink. Except for the volume transfer coupling, the twin and the parent ellipsoids are treated as independent inclusions in the model.

In the next section we critically test and calibrate the model using a comprehensive set of experimental data and provide new insights into the effect of deformation modes as a function of temperature and strain rate on the deformation behavior of  $\alpha$ -U.

#### 4. Results and discussion

The axial compression of polycrystalline aggregates of  $\alpha$ -U is simulated, over a wide range of temperatures and strain rates up to strain of 0.2, by imposing 0.002 strain increments along the IP and TT directions while enforcing zero average stress along the two lateral directions of the sample. We perform these simulations using the grain hardening model described above and a VPSC formulation for describing grain-matrix interaction. We represent the initial texture of Fig. 1 using 10,000 weighted orientations and we assign an initially spherical shape to the representative ellipsoids. As deformation proceeds and grains are split into parent and twin, oblate ellipsoidal shapes are assigned to the associated inclusions, and the total number of grains in the simulation increases. The VPSC formulation does not account for the elastic and the elasto-plastic portion of the mechanical response, which presents a difficulty because the  $\alpha$ -U response is characterized by an extended elasto-plastic transition upon loading. This long transition has been associated with the presence of large internal stresses in the uranium aggregate created during processing (Brown et al., 2009; Knezevic et al., 2012). In order to circumvent this issue, we devised a procedure based on the predictions of an elasto-plastic self-consistent model (Turner and Tomé, 1994) for estimating the strain associated with the end of the elasto-plastic transition. As a consequence, the VPSC predictions are shifted by the estimated strain at yield in order to compare them with the experimental stress-strain data. This procedure assumes that during the elasto-plastic transition there will be some twin nucleation induced by the slip activity. This is important

because our VPSC simulations allow twinning to start right from the beginning of the deformation and current theories (Christian and Mahajan, 1995; Knezevic et al., 2010; Wang et al., 2010) for the activation of deformation twinning rely on previous dislocation activity and stress concentrations at boundaries resulting from prior deformation. Details of this procedure were explained in our earlier work (Knezevic et al., 2012).

The hardening parameters were calibrated using a portion of the experimental data presented in the second section of this paper. The starting point for calibration were parameters from the earlier study (Knezevic et al., 2012) that were already good for the room temperature and quasi static predictions. We subsequently used four of the curves recorded at elevated temperatures and two of the curves recorded at high strain rates for the calibration. The remaining curves served to test model predictions. The hardening parameters for the slip modes and the twin modes are listed in Tables 1 and 2, respectively. Table 3 presents the variation of the shear modulus with temperature using third-order polynomials adjusted to the data given in Daniel et al. (1971) and Fisher and McSkimin (1958).

#### 4.1. Predicted response at room temperature under quasi-static loading

Fig. 3 compares the measured and predicted compressive stress–strain response in the three mutually perpendicular directions of the  $\alpha$ -U plate under quasi-static loading at room temperature. The measured stress–strain curves shown in Fig. 3 were reported in earlier studies (Knezevic et al., 2012; McCabe et al., 2010) and compared with the predictions of the hardening law reported in Knezevic et al. (2012). In that study we were concerned only with predicting the deformation behavior of  $\alpha$ -U at room temperature under quasi-static loading. In the present work, we extend the hardening law to account for strain-rate and temperature dependence. However, the revised hardening law should still reproduce the room temperature data under quasi-static loading conditions. Fig. 3 shows that the extended hardening law with the new hardening parameters successfully reproduces the measured mechanical response in all three directions IPC1, IPC2 and TTC3 for the

**Table 1**  
Slip mode hardening parameters.

	$\alpha = 1$ [100](010)	$\alpha = 2$ [100](001)	$\alpha = 3$ $\langle 1\bar{1}0 \rangle \{110\}$	$\alpha = 4$ $\langle 1\bar{1}2 \rangle \{021\}$
$b^z$ [nm]	$2.85 \times 10^{-1}$	$2.85 \times 10^{-1}$	$6.51 \times 10^{-1}$	$11.85 \times 10^{-1}$
$k_1^z$ [m $^{-1}$ ]	$2.35 \times 10^9$	$1.1 \times 10^7$	$6.0 \times 10^9$	$1.5 \times 10^8$
$\dot{\epsilon}_0^z$ [s $^{-1}$ ]	$10^7$	$10^7$	$10^7$	$10^7$
$g^z$	$5.2 \times 10^{-4}$	$3.2 \times 10^{-4}$	$7.0 \times 10^{-4}$	$4.0 \times 10^{-3}$
$D_0^z$ [MPa]	41	88	50	72
$q^z$	$28 \exp\left(-\frac{T-295}{500}\right)$	0	$4.8 \exp\left(-\frac{T-295}{500}\right)$	$80 \exp\left(-\frac{T-295}{500}\right)$
$\tau_0^z$ [MPa]	$185 \exp\left(-\frac{T-295}{250}\right)$	$395 \exp\left(-\frac{T-295}{230}\right)$	$500 \exp\left(-\frac{T-295}{160}\right)$	$600 \exp\left(-\frac{T-295}{1000}\right)$
$\chi^{\alpha\alpha'}$ , $\alpha' = 1$	1.7	2.0	2.0	1
$\chi^{\alpha\alpha'}$ , $\alpha' = 2$	2.0	1.7	2.0	1
$\chi^{\alpha\alpha'}$ , $\alpha' = 3$	2.0	2.0	1.7	1
$\chi^{\alpha\alpha'}$ , $\alpha' = 4$	2.0	2.0	2.0	.95

**Table 2**  
Twin mode hardening parameters.

	$\beta = 1$ {130} (3 $\bar{1}$ 0)	$\beta = 2$ {172} (3 $\bar{1}$ 2)
$\tau_0^z$ [MPa]	100	240
$C^{\alpha\beta}$ , $\alpha = 1$	$5500 \exp\left(\frac{\dot{\epsilon}-0.001}{400}\right)$	$5500 \exp\left(\frac{\dot{\epsilon}-0.001}{400}\right)$
$C^{\alpha\beta}$ , $\alpha = 2$	$500 \exp\left(\frac{\dot{\epsilon}-0.001}{1000}\right)$	$500 \exp\left(\frac{\dot{\epsilon}-0.001}{1000}\right)$
$C^{\alpha\beta}$ , $\alpha = 3$	$7500 \exp\left(\frac{\dot{\epsilon}-0.001}{1000}\right)$	$7500 \exp\left(\frac{\dot{\epsilon}-0.001}{1000}\right)$
$C^{\alpha\beta}$ , $\alpha = 4$	$7800 \exp\left(\frac{\dot{\epsilon}-0.001}{400}\right)$	$3100 \exp\left(\frac{\dot{\epsilon}-0.001}{400}\right)$
$b^\beta$ [nm]	0.1036	1.433

**Table 3**  
Shear modulus [MPa].

$\alpha = 1$ [100](010)	$4.710 \times 10^{-5}T^3 - 0.099T^2 + 1.174T + 8.295 \times 10^4$
$\alpha = 2$ [100](001)	$7.319 \times 10^{-5}T^3 - 0.121T^2 - 23.852T + 9.103 \times 10^4$
$\alpha = 3$ $\langle 1\bar{1}0 \rangle \{110\}$	$5.036 \times 10^{-5}T^3 - 0.108T^2 + 22.368T + 7.546 \times 10^4$
$\alpha = 4$ $\langle 1\bar{1}2 \rangle \{021\}$	$-6.087 \times 10^{-5}T^3 + 0.062T^2 - 49.349T + 7.926 \times 10^4$
$\beta = 1$ {130} (3 $\bar{1}$ 0)	$74 \times 10^3$
$\beta = 2$ {172} (3 $\bar{1}$ 2)	$74 \times 10^3$

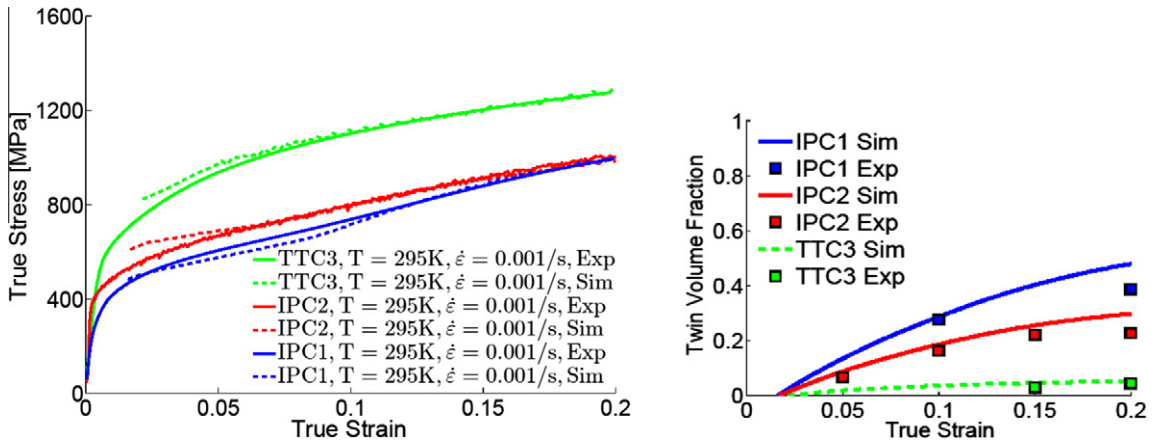


**Fig. 3.** Simple compression response of  $\alpha$ -uranium corresponding to the compression directions, temperature and strain rate indicated in the plots. Measured and predicted true stress-true strain responses are depicted as solid and dashed lines, respectively. The right panel shows the evolution of {130} twin volume fractions in the samples, as predicted by VPSC (lines) and measured by EBSD (symbols), as a function of strain.

given loading conditions. In particular, the model captures the characteristic increase in the hardening rate associated with twinning activity for the in-plane deformation cases. We note the concave shape of the IPC1 true stress – true strain response, where the twin volume fraction reaches over 50%. The EBSD analysis performed in our earlier Knezevic et al. (2012) work shows that the twin volume fraction of {130} twin is far greater than that of {172} twin. The twin resistances of {130} and {172} twins are predicted to be 100 and 280 MPa, respectively. Also, the {130} twin appears to be the softest deformation mode in  $\alpha$ -U. The predicted and measured evolution of {130} twin volume fractions are compared in Fig. 3 for the three samples. We find good agreement between the experimental and simulated twin volume fractions. In Fig. 4 we compare the measured and predicted textures for 0.2 strain and we find that the model captures well the texture evolution in all three cases.

An accurate prediction of the mechanical response and texture evolution is an indication that the predicted relative activities of the slip and twin modes contributing to plastic deformation is correct. Contributions to shear per mode are normalized by the total contribution of all slip and twinning modes, as follows:

$$\text{RelActMode}^m = \frac{\sum_{s_m} \dot{\gamma}^{s_m}}{\sum_{m'} \sum_{s_{m'}} \dot{\gamma}^{s_{m'}}}. \quad (14)$$

The relative activity plots corresponding to the room temperature quasi-static deformation conditions are shown in Fig. 5, where we illustrate both the mode activity within the parent material and the mode activity within the twinned material. The predicted deformation modes for the IP deformation show substantial activity of deformation twinning in the parent

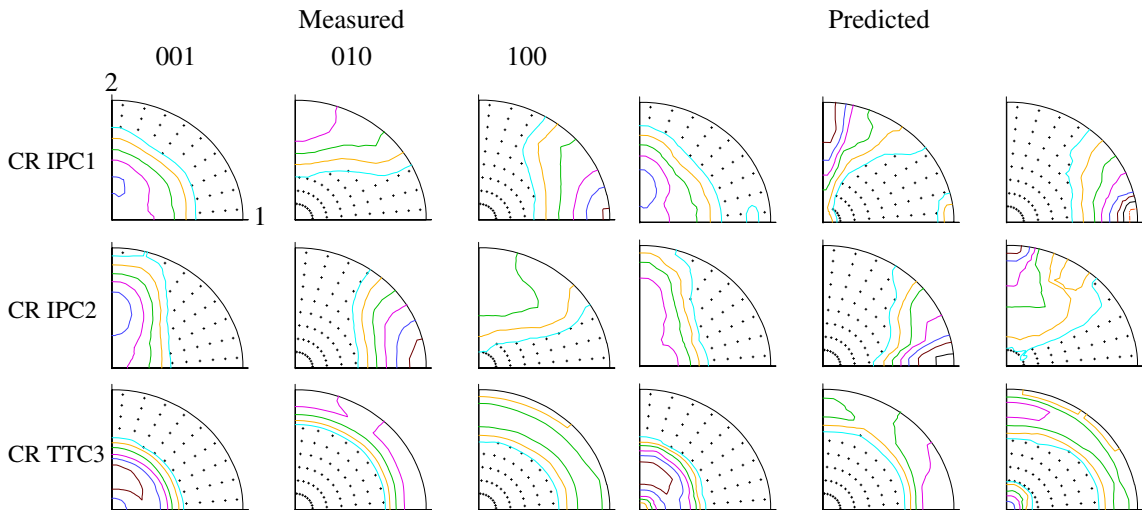


**Fig. 4.** Pole figures showing measured (on the left) and predicted (on the right) textures for 0.2 strain in the  $\alpha$ -U samples deformed at room temperature and at a strain rate of  $0.001 \text{ s}^{-1}$  along the indicated directions. The intensity of the contour lines is 0.7/1.0/1.4/2.0/2.8/4.0/5.7/8. The IP1 and IP2 directions are indicated by the 1 and 2 on the pole figures.

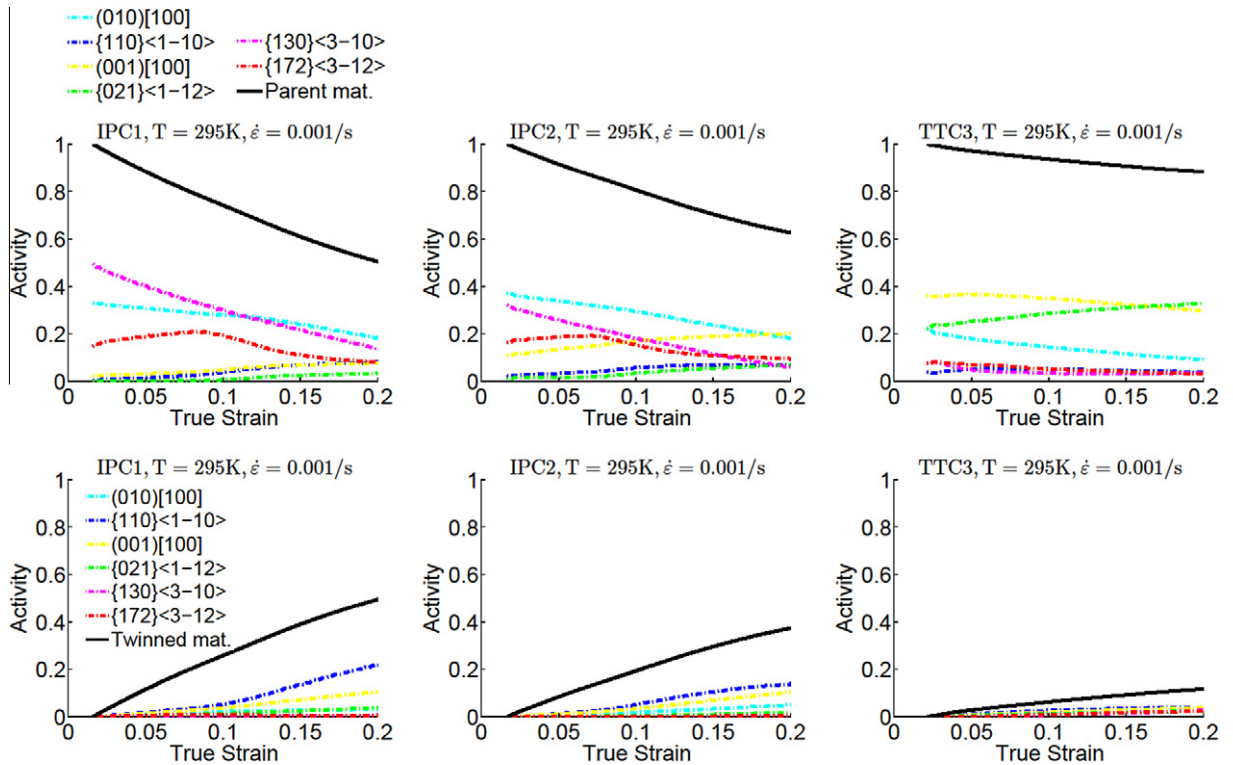


**Fig. 5.** Predicted relative activities of each deformation mode contributing to plasticity in both parent (top row) and twin (bottom row) phases for the samples described in Fig. 3. Also plotted are the predicted parent (top row) and twin (bottom row) volume fractions.

material. Deformation of the twinned domains requires activation of secondary slip involving the relatively hard  $\{110\}\langle 1\bar{1}0\rangle$  mode, and thus more hardening. The IPC2 activity plots also show substantial activity of the  $(010)[100]$  slip. This kind of slip in combination with  $\{110\}\langle 1\bar{1}0\rangle$  form slip bands, as reported in Knezevic et al. (2012). The fact that dislocations in  $\alpha$ -U organize and form substructures is reflected in our model by the nonzero values of  $q(T)$  (see Table 1). This factor defines the fraction of dislocations leading to debris formation. It is predicted that TT plastic deformation is mainly accommodated by the  $(001)[100]$ ,  $(010)[100]$  and  $\{021\}\langle 1\bar{1}2\rangle$  slip modes. Activation of all slip modes can be rationalized by the low number of glide systems per mode available in  $\alpha$ -U. During the TT deformation and after 0.2 strain less than 10% of the volume was reoriented by twinning, and little texture evolution occurs (see Fig. 4).

#### 4.2. Predicted response at elevated temperatures under quasi-static loading

Fig. 6 shows the comparison between the measured and predicted stress–strain response of  $\alpha$ -U samples subject to TT quasi-static compression at various temperatures, together with the predicted texture at 0.2 strain. The predicted relative deformation mode activities are depicted in Fig. 7, and show a qualitative change with respect to room temperature. The predominant slip systems have changed and twinning is nearly suppressed. The  $(001)[100]$  slip becomes softer and predominant with temperature, consistent with earlier measurements on single crystals (Daniel et al., 1971) as well as theoretical predictions (Yoo, 1968). It is observed experimentally, as well as predicted by our model, that a small fraction of plastic deformation is accommodated by twinning during TT compression. The model predicts that this fraction decreases with increasing temperature, consistent with a number of earlier studies on deformation twinning involving many material systems. The decrease in the yield stress and the hardening rate with temperature during TT compression is the consequence of thermally-activated slip processes. Our analysis shows that the  $(010)[100]$  slip is relatively temperature insensitive. The  $(001)[100]$  slip is more temperature sensitive and a large fraction of grains are oriented well for this deformation mode resulting in an increase in  $(001)[100]$  activity and a decrease in flow stress. The  $\{110\}\langle 1\bar{1}0\rangle$  and  $\{021\}\langle 1\bar{1}2\rangle$  slip modes also exhibit temperature sensitivity, but few grains are oriented well for  $\{110\}\langle 1\bar{1}0\rangle$  slip during TT compression and  $\{021\}\langle 1\bar{1}2\rangle$  remains much more difficult to activate than  $(001)[100]$  slip at the tested temperatures. As is to be expected, the amount of dynamic recovery increases with temperature, which is reflected by the exponential decay of  $q(T)$  in our model. Still, the recovery is not sufficient at 473 and 573 K to cancel out the build up of debris and to predict the observed saturation of the flow stress (see Fig 6). The predicted change in texture with temperature is not substantial. The enhancement in the  $(010)$  component along the IP1 direction and of the  $(100)$  component near the IP2 direction result from the increased amount of  $(001)[100]$  slip activity.

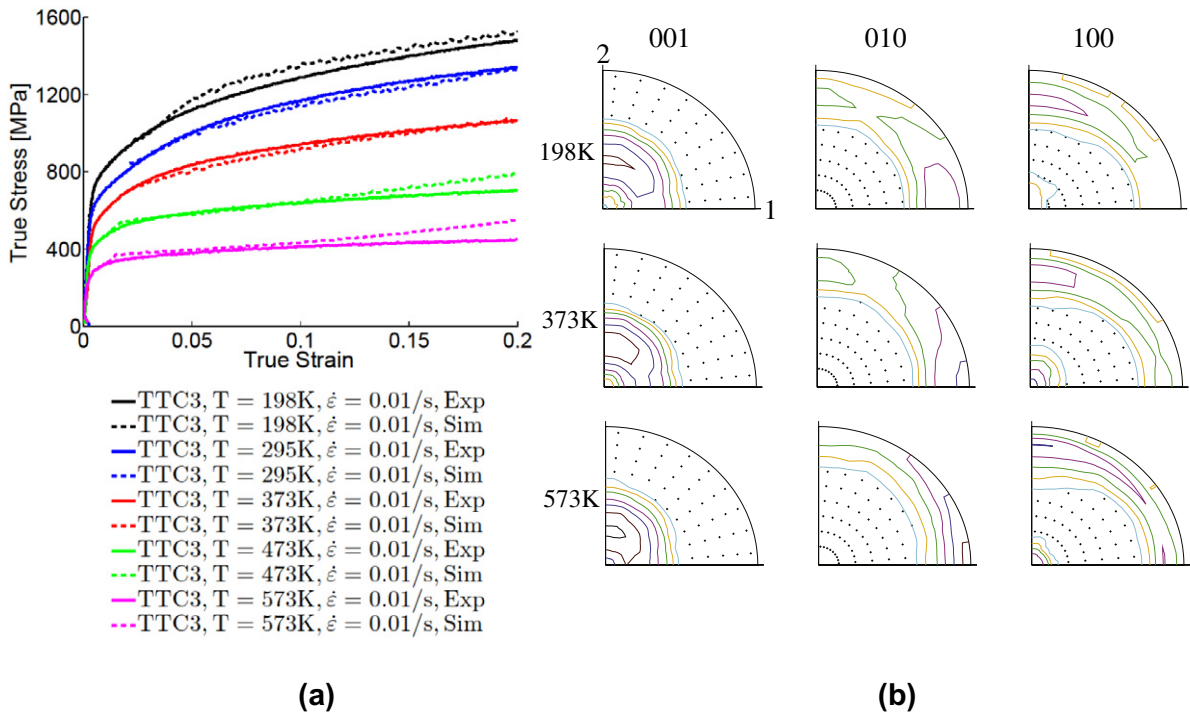


**Fig. 6.** Temperature effect on the through-thickness mechanical response and texture evolution of  $\alpha$ -uranium. (a) Measured and predicted true stress-true strain responses are depicted as solid and dashed lines, respectively. (b) Pole figures showing predicted textures at a 0.2 strain. The intensity of the contour lines is 0.7/1.0/1.4/2.0/2.8/4.0/5.7/8. The IP1 and IP2 directions are indicated by the 1 and 2 on the pole figures.

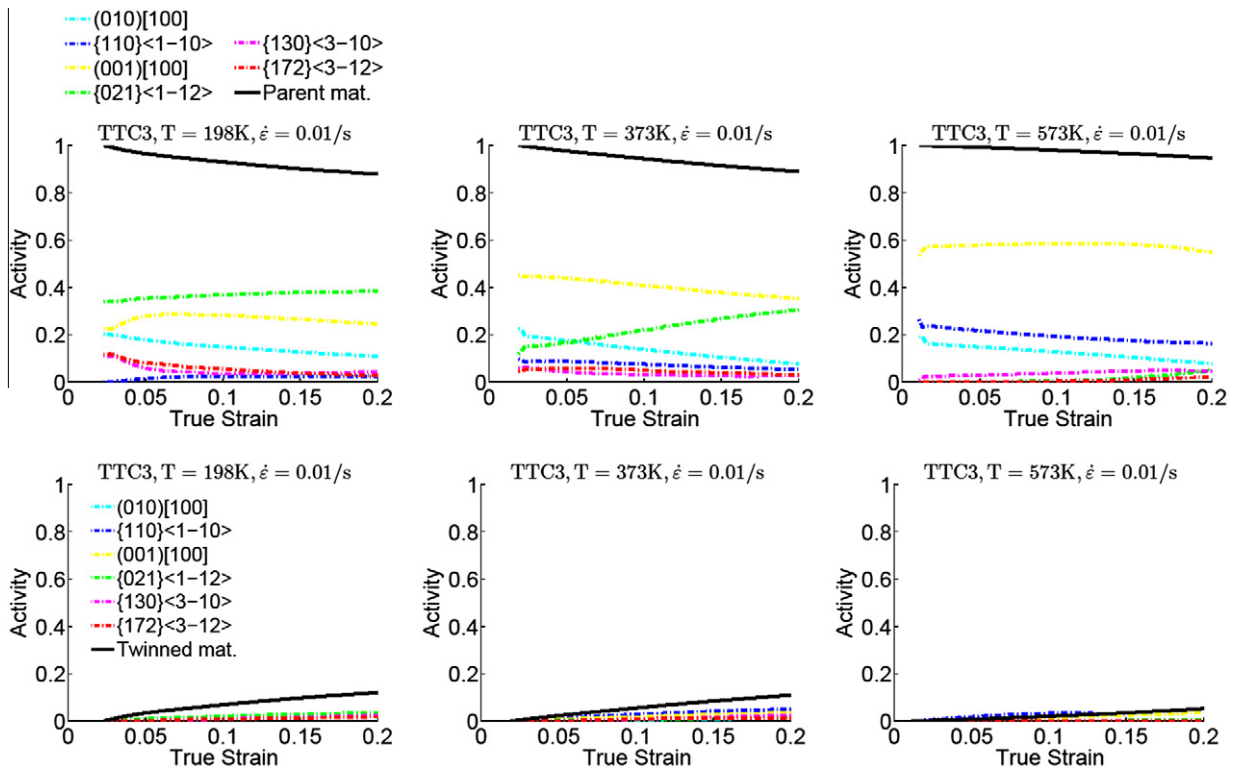


**Fig. 7.** Predicted relative activities of each deformation mode contributing to plasticity in both parent (top row) and twin (bottom row) phases for samples compressed in the through-thickness direction at various temperatures (see Fig. 6). Also plotted are the predicted parent (top row) and twin (bottom row) volume fractions.

In Fig. 8 we compare measured and predicted stress–strain response of  $\alpha$ -U subjected to IP quasi-static compression at various temperatures. A noticeable transition in the hardening rate is observed in the IP response as the temperature decreases from 573 to 198 K. Based on our model results, this transition is correlated with a transition from slip-dominated deformation at 573 K to an increased activity of twinning and more difficult activation of thermally-activated slip modes as the temperature decreases (see Fig. 9). An increasing twin volume fraction is predicted in the IPC2 sample (over 40% at 0.2 strain at 198 K). While growing and accommodating plastic strain, deformation twins reorient grains to harder orientations, thus inducing texture hardening (Knezevic et al., 2012; McCabe et al., 2010). The model explicitly accounts for the texture hardening by reorienting the grains. In addition, the strain hardening increases due to the propagation of the twin interface into a domain containing dislocations (Basinski et al., 1997). We account for these effects empirically in our model via the latent hardening matrix. The increase of strain hardening rate could also arise from grain subdivision associated with twinning (Asgari et al., 1997; Proust et al., 2009, 2007), a Hall–Petch-like effect. However, in the case of  $\alpha$ -U twins grow at fast rates and readily consume entire grains. Therefore the Hall–Petch-like hardening effect is not expected to be significant in  $\alpha$ -U (Knezevic et al., 2012, 2010) and is not accounted for in our model. The fact that the model captures quite well the highly anisotropic mechanical behavior of  $\alpha$ -uranium confirms our reasoning. The activation of hard slip within twinned volumes (referred to as the secondary slip) is also relevant for hardening mainly at lower temperatures.

Fig. 8(b) shows the predicted change in texture with temperature for the IP compressed samples along axis 2 (IPC2). The (130) twinning results in shifts of the (010) and (100) intensities towards the IP1 and IP2 directions, respectively. The sharpness of these peaks increases with increasing temperature mainly due to increased activity of  $\{110\}\langle 110\rangle$  dislocations with increasing temperature. The spread of the (001) intensity towards the compression direction IP2 increases with decreasing temperature and this change in texture requires more activity of hard  $\{021\}\langle 112\rangle$  slip.

#### 4.3. Predicted response at room temperature under high-strain-rate loading

Fig. 10 shows the comparison between measured and predicted stress–strain curves and textures at 0.2 strain in  $\alpha$ -U samples subject to IP and TT high strain-rate deformation at room temperature. In order to allow for the comparison between high strain-rate and quasi-static deformation conditions, we also show the quasi-static response. The work hardening rate during both the IP and TT compression is higher at high strain-rate in the early portion of the stress–strain curves relative to the quasi-static loading conditions. While the hardening rate of the IP curve continues to be higher with straining, the TT hardening tends to saturate faster with the rate of deformation. As seen earlier, the TT deformation is dominated by thermally-activated slip, which is more difficult to activate with increasing strain rates. Therefore, the yield stress in the TT case increases with the rate of deformation. On the other hand, the initial macroscopic yield stress appears insensitive to the rate of deformation in IP compression. We associate this with twinning, which is the easiest deformation mode in  $\alpha$ -U. In the IP case, the origin of the monotonic increase in the hardening rate under higher strain-rate relative to the quasi-static conditions is a combination of more difficult thermally-activated slip and stronger slip–twin interactions. The values of the latent

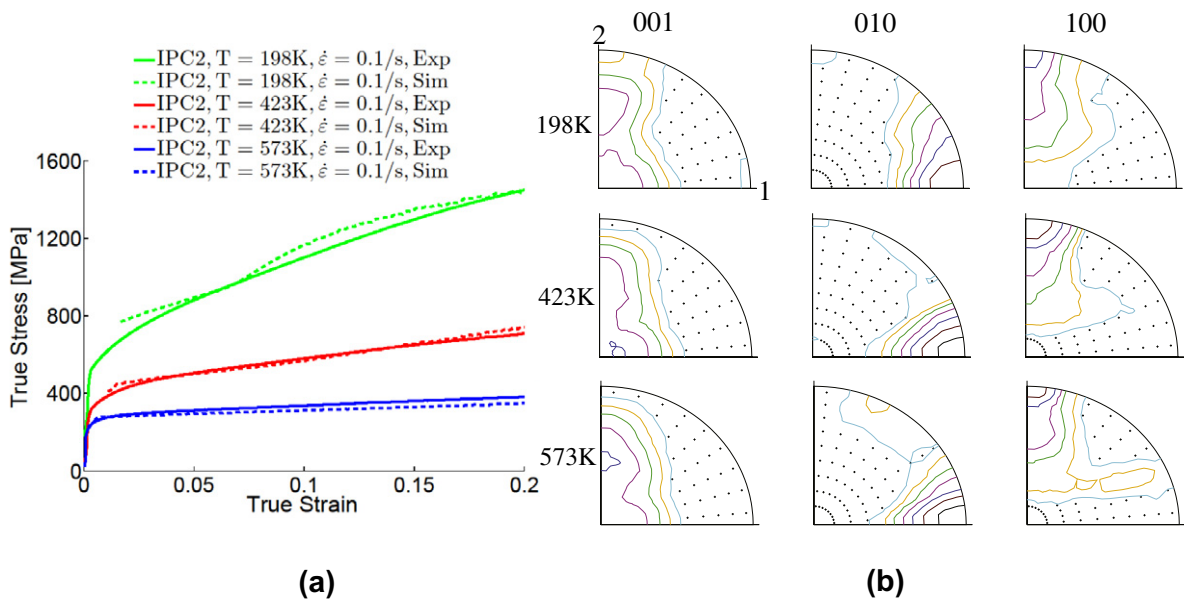


**Fig. 8.** Temperature effect on the in-plane mechanical response and texture evolution of  $\alpha$ -uranium. (a) Measured and predicted true stress–true strain responses are depicted as solid and dashed lines, respectively. (b) Pole figures showing predicted textures at 0.2 strain. The intensity of the contour lines is 0.7/1.0/1.4/2.0/2.8/4.0/5.7/8. The IP1 and IP2 directions are indicated by the 1 and 2 on the pole figures.

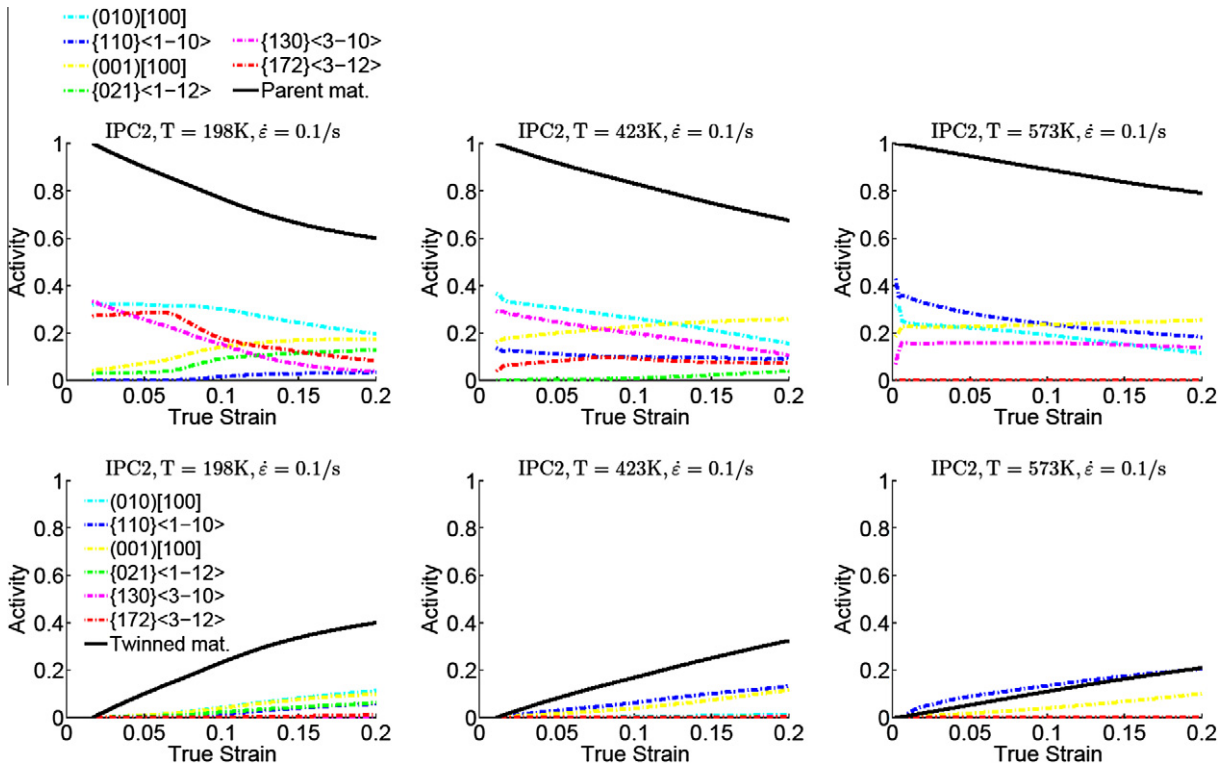


**Fig. 9.** Predicted relative activities of each deformation mode contributing to plasticity in both parent (top row) and twin (bottom row) phases for samples compressed in the in-plane two direction at various temperatures (see Fig. 8). Also plotted are the predicted parent (top row) and twin (bottom row) volume fractions.

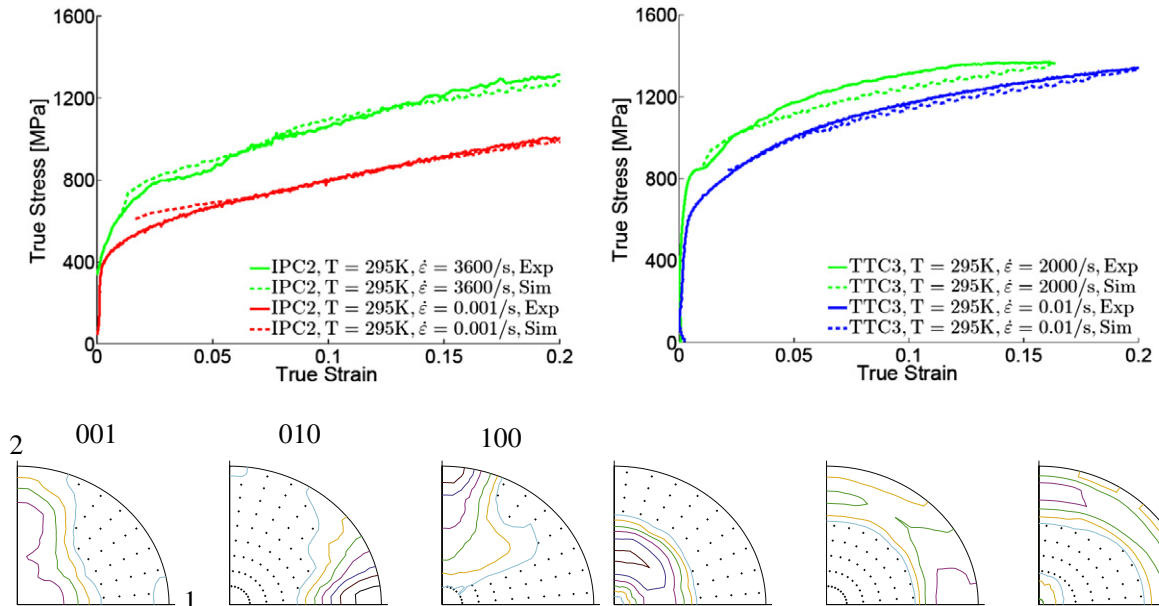


**Fig. 10.** Strain-rate effect on the mechanical response and texture evolution of  $\alpha$ -uranium. Measured and predicted true stress-true strain responses are depicted as solid and dashed lines, respectively, for in-plane compression (on the left) and through-thickness compression (on the right). The pole figures showing predicted textures at strain of 0.2 under the high rate deformation for in-plane compression (on the left) and through-thickness compression (on the right). The intensity of the contour lines is 0.7/1.0/1.4/2.0/2.8/4.0/5.7/8. The IP1 and IP2 directions are indicated by the 1 and 2 on the pole figures.

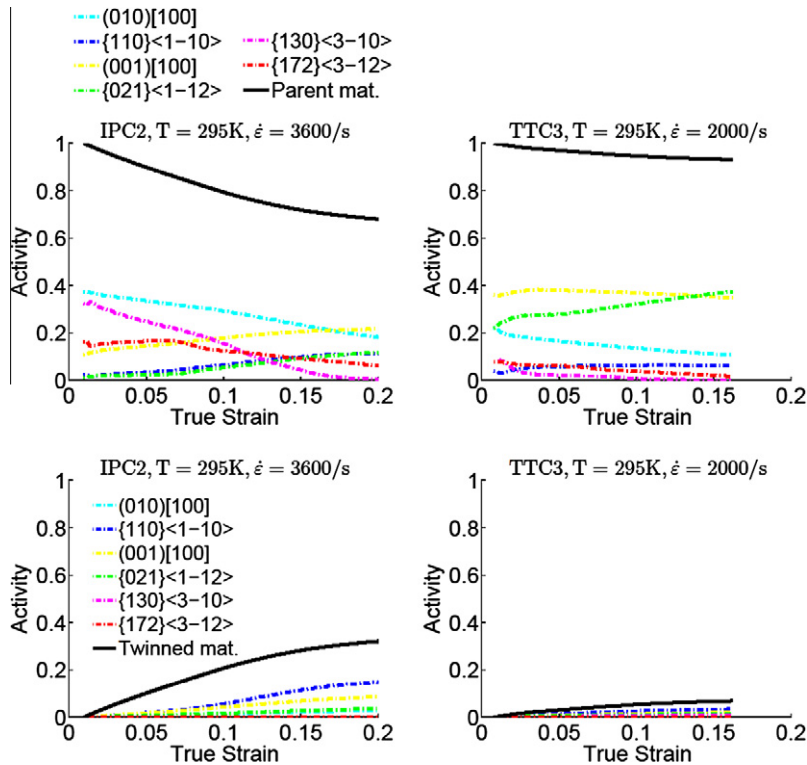


**Fig. 11.** Predicted relative activities of each deformation mode contributing to plasticity in the parent (top row) and the twin (bottom row) phases for samples compressed at various strain rates (see Fig. 10). Also plotted are the predicted parent material (top row) and twinned material (bottom row) volume fractions.

hardening matrix are reported in Table 2. The hardening coming from twinning and how it is accounted for in our model was discussed in the previous section. In addition to those effects, we reduce by 50% the thickness of the twin lamella for the high strain rate deformation relative to the quasi-static deformation. We note that the shape and orientation of the twin ellipsoids is accounted for in the self-consistent equations and this affects the macroscopic response. Although the twin volume fractions are not predicted to increase significantly with the deformation rate, we assumed that the morphological features of twins vary with the deformation rate (Song and Gray 1995a), thus influencing the macroscopic hardening. Otherwise, the predicted relative contribution of active deformation modes (see Fig. 11) and texture do not appear to vary appreciably with the deformation rate.

## 5. Conclusions

In this paper we present a polycrystal-plasticity-based model able to predict the mechanical response and texture evolution of  $\alpha$ -uranium over a wide range of temperatures and strain rates. This model is based on a self-consistent homogenization of the single crystal responses and allows for a detailed comparison with macroscopic measurements. The hardening of individual crystals is based on the evolution of dislocation densities and includes effects of strain rate and temperature through the thermally-activated recovery and substructure formation of dislocation slip and through slip-twin interactions. The model is tested on a comprehensive set of measured stress–strain data recorded for a wide range of temperatures and under different strain rates along the through-thickness and in-plane directions of a clock-rolled  $\alpha$ -uranium plate. We show that the model is able to reproduce the stress–strain response for all tests with a unique set of single-crystal hardening parameters. We regard the predictive capabilities of the model as reliable for monotonic loading. The good modeling results represent a significant incentive for incorporating the present VPSC-based constitutive model of uranium into finite-element frameworks (Knezevic et al., 2009; Segurado et al., 2012) and microstructure sensitive design frameworks (Fast et al., 2008; Knezevic and Kalidindi, 2007; Knezevic et al., 2008a, 2008b; Shaffer et al., 2010).

Based on our model predictions, we quantify the role of deformation modes on the mechanical behavior and texture evolution in  $\alpha$ -uranium. The through-thickness deformation is dominated by dislocation slip with transition from the harder  $\{021\}\langle 1\bar{1}2 \rangle$  slip to the softer  $(001)[100]$  slip with temperature. Macroscopic initial yield stress, as well as strain hardening, is sensitive to the rate of deformation in through-thickness compression. The yield stress increases due to a greater difficulty in the activation of slip at higher strain rates. After the thermally-activated slip is activated, the hardening rate decreases

leading to faster saturation at high strain-rate relative to the quasi-static strain-rate conditions. Texture evolution appears to be insensitive to both temperature and strain rate during through-thickness compression. The in-plane response of  $\alpha$ -uranium exhibits a noticeable transition in hardening as temperature decreases from 573 to 198 K. This transition is associated with the transition from slip-dominated deformation at 573 K to an increasing activity of twinning and more difficult activation of thermally-activated slip modes as the temperature decreases. The initial macroscopic yield stress appears insensitive to the rate of deformation in the case of in-plane compression. We associate this with (130) twinning, which is the easiest deformation mode in  $\alpha$ -U. The volume fraction of twinned material reaches 50% for 0.2 strain and does not appear to vary with strain rate. The origin of the continuing increase in the hardening rate under higher strain rate relative to the quasi-static conditions is a combination of more difficult thermally-activated slip and stronger slip-twin interactions. The strain hardening rate at 573 K, where thermally-activated processes become easy, is seen to be texture insensitive under the quasi-static responses and both the in-plane and through-thickness curves exhibit similar and approximately constant work hardening rates.

## Acknowledgments

This work was performed under contract number DE-AC52-06NA25396 with the US Department of Energy. Marko Knezevic gratefully acknowledges the Seaborg Institute for the Post-Doctoral Fellowship through the LANL/LDRD Program with the U.S. Department of Energy.

## References

- Anderson, R.G., Bishop, J.W., 1962. The effect of neutron irradiation and thermal cycling on permanent deformations in uranium under load. The Institute of Metals, London, pp. 17–23.
- Asgari, S., El-Danaf, E., Kalidindi, S.R., Doherty, R.D., 1997. Strain hardening regimes and microstructural evolution during large strain compression of low stacking fault energy FCC alloys that form deformation twins. *Metallurgical and Materials Transactions A: Physical Metallurgy and Materials Science* 28A (9), 1781–1795.
- Barnett, M.R., 2001. Influence of deformation conditions and texture on the high temperature flow stress of magnesium AZ31. *Journal of Light Metals* 1 (3), 167–177.
- Basinski, Z.S., 1960. The influence of temperature and strain rate on the flow stress of magnesium single crystals. *Australian Journal of Physics* 13, 284–298.
- Basinski, Z.S., Szczerba, M.S., Niewczas, M., Embury, J.D., Basinski, S.J., 1997. Transformation of slip dislocations during twinning of copper-aluminum alloy crystals. *Revue de Metallurgie. Cahiers D'Informations Techniques* 94 (9), 1037–1044.
- Beyerlein, I.J., Tomé, C.N., 2008. A dislocation-based constitutive law for pure Zr including temperature effects. *International Journal of Plasticity* 24 (5), 867–895.
- Brown, D.W., Beyerlein, I.J., Sisneros, T.A., Clausen, B., Tomé, C.N., 2012. Role of twinning and slip during compressive deformation of beryllium as a function of strain rate. *International Journal of Plasticity* 29, 120–135.
- Brown, D.W., Bourke, M.A.M., Clausen, B., Korzekwa, D.R., Korzekwa, R.C., McCabe, R.J., Sisneros, T.A., Teter, D.F., 2009. Temperature and direction dependence of internal strain and texture evolution during deformation of uranium. *Materials Science and Engineering: A* 512 (1–2), 67–75.
- Cahn, R.W., 1951. Twinning and slip in  $\alpha$ -uranium. *Acta Crystallographica* 4 (5), 470.
- Cahn, R.W., 1953. Plastic deformation of alpha-uranium, twinning and slip. *Acta Metallurgica* 1 (1), 49–52, IN1–IN5, 53–70.
- Calnan, E.A., Clews, C.J.B., 1952. The prediction of uranium deformation textures. *Philosophical Magazine Series 7* 43 (336), 93–104.
- Chen, S.R., Kocks, U.F., 1991. High-temperature plasticity in copper polycrystals. *High Temperature Constitutive Modeling Theory and Application*, 1–21.
- Choi, C.S., Staker, M., 1996. Neutron diffraction texture study of deformed uranium plates. *Journal of Materials Science* 31 (13), 3397–3402.
- Christian, J.W., Mahajan, S., 1995. Deformation twinning. *Progress in Materials Science* 39 (1–2), 1–157.
- Crocker, A.G., 1965. The crystallography of deformation twinning in alpha-uranium. *Journal of Nuclear Materials* 16 (3), 306–326.
- Daniel, J.S., Lesage, B., Lacombe, P., 1971. The influence of temperature on slip and twinning in uranium. *Acta Metallurgica* 19 (2), 163–173.
- Fast, T., Knezevic, M., Kalidindi, S.R., 2008. Application of microstructure sensitive design to structural components produced from hexagonal polycrystalline metals. *Computational Materials Science* 43 (2), 374–383.
- Fisher, E.S., McSkimin, H.J., 1958. Adiabatic elastic moduli of single crystal alpha Uranium. *Journal of Applied Physics* 29 (10), 1473–1484.
- Flynn, P.W., Motte, J., Dorn, J.E., 1961. On the thermally activated, mechanism of prismatic slip in magnesium single crystals. *Transactions of the Metallurgical Society of the American Institute of Mechanical Engineers* 221, 1148–1154.
- Follansbee, P.S., 1985. High Strain Rate Compression Testing – The Hopkinson Bar, ninth ed. Am. Soc. Metals, Metals Park, Ohio, vol. 8, pp. 198–203.
- Gray III, G.T., 1997. Influence of strain rate and temperature on the structure-property behavior of high-purity titanium. *Journal De Physique IV* 7, 423–428.
- Knezevic, M., Al-Harbi, H.F., Kalidindi, S.R., 2009. Crystal plasticity simulations using discrete Fourier transforms. *Acta Materialia* 57 (6), 1777–1784.
- Knezevic, M., Capolungo, L., Tomé, C.N., Lebensohn, R.A., Alexander, D.J., Mihaila, B., McCabe, R.J., 2012. Anisotropic stress-strain response and microstructure evolution of textured  $\alpha$ -uranium. *Acta Materialia* 60 (2), 702–715.
- Knezevic, M., Kalidindi, S.R., 2007. Fast computation of first-order elastic-plastic closures for polycrystalline cubic-orthorhombic microstructures. *Computational Materials Science* 39 (3), 643–648.
- Knezevic, M., Kalidindi, S.R., Fullwood, D., 2008a. Computationally efficient database and spectral interpolation for fully plastic Taylor-type crystal plasticity calculations of face-centered cubic polycrystals. *International Journal of Plasticity* 24 (7), 1264–1276.
- Knezevic, M., Kalidindi, S.R., Mishra, R.K., 2008b. Delineation of first-order closures for plastic properties requiring explicit consideration of strain hardening and crystallographic texture evolution. *International Journal of Plasticity* 24 (2), 327–342.
- Knezevic, M., Levinson, A., Harris, R., Mishra, R.K., Doherty, R.D., Kalidindi, S.R., 2010. Deformation twinning in AZ31: influence on strain hardening and texture evolution. *Acta Materialia* 58 (19), 6230–6242.
- Lavrentev, F.F., 1980. The type of dislocation interaction as the factor determining work hardening. *Materials Science and Engineering* 46 (2), 191–208.
- Lebensohn, R.A., Tomé, C.N., 1993. A self-consistent anisotropic approach for the simulation of plastic deformation and texture development of polycrystals: application to zirconium alloys. *Acta Metallurgica et Materialia* 41 (9), 2611–2624.
- Lebensohn, R.A., Tomé, C.N., 1994. A self-consistent viscoplastic model: prediction of rolling textures of anisotropic polycrystals. *Materials Science and Engineering: A* 175 (1–2), 71–82.
- Lebensohn, R.A., Tomé, C.N., Castaneda, P.P., 2007. Self-consistent modelling of the mechanical behaviour of viscoplastic polycrystals incorporating intragranular field fluctuations. *Philosophical Magazine* 87 (28), 4287–4322.
- Mader, R., Devincere, B., Kubin, L.P., 2002. From dislocation junctions to forest hardening. *Physical Review Letters* 89 (25), 255508.
- McCabe, R.J., Capolungo, L., Marshall, P.E., Cady, C.M., Tomé, C.N., 2010. Deformation of wrought uranium: experiments and modeling. *Acta Materialia* 58 (16), 5447–5459.

- McCabe, R.J., Teter, D.F., 2006. Analysis of recrystallized volume fractions in uranium using electron backscatter diffraction. *Journal of Microscopy* 223 (1), 33–39.
- Mitchell, C.M., Rowland, J.F., 1954. Preferred orientation in  $\alpha$ -uranium. *Acta Metallurgica* 2 (4), 559–572.
- Proust, G., Tomé, C.N., Jain, A., Agnew, S.R., 2009. Modeling the effect of twinning and detwinning during strain-path changes of magnesium alloy AZ31. *International Journal of Plasticity* 25 (5), 861–880.
- Proust, G., Tomé, C.N., Kaschner, G.C., 2007. Modeling texture, twinning and hardening evolution during deformation of hexagonal materials. *Acta Materialia* 55 (6), 2137–2148.
- Rollett, A.D., 1991. Comparison of experimental and theoretical texture development in alpha-uranium. In: Lowe, T.C., Rollett, A.D., Follansbee, P.S., Daehn, G.S. (Eds.), Warrendale, PA, pp. 361–368.
- Segurado, J., Lebensohn, R.A., Llorca, J., Tomé, C.N., 2012. Multiscale modeling of plasticity based on embedding the viscoplastic self-consistent formulation in implicit finite elements. *International Journal of Plasticity* 28 (1), 124–140.
- Shaffer, J.B., Knezevic, M., Kalidindi, S.R., 2010. Building texture evolution networks for deformation processing of polycrystalline fcc metals using spectral approaches: applications to process design for targeted performance. *International Journal of Plasticity* 26 (8), 1183–1194.
- Song, S., Gray, G., 1995a. Influence of temperature and strain rate on slip and twinning behavior of Zr. *Metallurgical and Materials Transactions A* 26 (10), 2665–2675.
- Song, S.G., Gray III, G.T., 1995b. Structural interpretation of the nucleation and growth of deformation twins in Zr and Ti-II. Tem study of twin morphology and defect reactions during twinning. *Acta Metallurgica et Materialia* 43 (6), 2339–2350.
- Turner, P.A., Tomé, C.N., 1994. A study of residual stresses in Zircaloy-2 with rod texture. *Acta Metallurgica et Materialia* 42 (12), 4143–4153.
- Van Houtte, P., 1978. Simulation of the rolling and shear texture of brass by the Taylor theory adapted for mechanical twinning. *Acta Metallurgica et Materialia* 26 (4), 591–604.
- Wang, J., Beyerlein, I.J., Tomé, C.N., 2010. An atomic and probabilistic perspective on twin nucleation in Mg. *Scripta Materialia* 63 (7), 741–746.
- Yoo, M.H., 1968. Slip modes of alpha uranium. *Journal of Nuclear Materials* 26 (3), 307–318.